

Heteroepitaxial growth of Co/Cu(001): An accelerated molecular dynamics simulation study

Radu A. Miron

Fritz-Haber-Institut der Max-Planck-Gesellschaft, Faradayweg 4-6, D-14195 Berlin-Dahlem, Germany

Kristen A. Fichthorn

Departments of Chemical Engineering and Physics, Pennsylvania State University, University Park, Pennsylvania 16802, USA

(Received 28 December 2004; revised manuscript received 15 April 2005; published 6 July 2005)

We employ static energy calculations and accelerated molecular dynamics (MD) simulations to study atomistic processes involved in the growth of Co on Cu(001) surfaces. The system is modeled with an empirical tight-binding (second-moment approximation) potential. Our accelerated MD algorithm, which detects, on the fly, groups of states connected by small barriers and consolidates them into larger states, allows us to reach time scales of seconds close to room temperature. These capabilities enable direct comparison to kinetic Monte Carlo and experimental studies of the initial stages of Co/Cu(001) growth. We observe upward interlayer transport mechanisms that contribute to bilayer island formation at low surface temperatures. At high temperatures the mixing of Co into the surface produces qualitative changes in the island structure, leading to the reversal of the low-temperature transport mechanisms and resulting in monolayer growth. We find that small Co islands can be as mobile as single adatoms and that they significantly affect the low-coverage morphology.

DOI: [10.1103/PhysRevB.72.035415](https://doi.org/10.1103/PhysRevB.72.035415)

PACS number(s): 68.55.Ac, 81.15.Aa

I. INTRODUCTION

Heteroepitaxial thin-film growth of Co on Cu substrates has been studied extensively during the last decade. Systems consisting of thin Co/Cu layers exhibit interesting properties stemming from reduced dimensionality, strained atomic structure, and magnetic interlayer coupling. Electronic properties of heteroepitaxial thin-film structures are very sensitive to their atomic-scale morphology, hence the importance of accurate characterization of the growth morphology. At room temperature, Co crystallizes into the hcp structure,¹ whereas Cu has an fcc structure.² However, Co grows pseudomorphically, in a fcc structure on the Cu substrate up to 20 monolayers.³ Although the lattice mismatch is only about 2%, this can significantly affect kinetic processes.^{4,5} The surface free energy of Co is larger than the Cu surface free energy,^{3,6} and the heat of mixing for bulk Cu—Co is endothermic.⁷ Using density-functional theory (DFT) calculations, Pentcheva and others analyzed possible equilibrium structures for a monolayer coverage of Co on Cu(001).^{6,8} Based on purely energetic considerations, a flat Co film on top of the Cu(001) substrate is the least stable structure, whereas the preferred structure was found to be a bilayer-high Co island capped by a Cu layer. However, since growth is a nonequilibrium process, the actual morphology is determined by the kinetic processes that are active on the deposition time scale.

Experimental studies reveal a variety of growth modes. At temperatures below room temperature, the preferred growth mode consists of bilayer-thick Co islands up to 2 ML, followed by layer-by-layer growth for the following layers.^{3,9,10} Kief and Egelhoff³ find that growth at $F=0.033$ ML/s and $T=80-300$ K proceeds through nucleation of bilayer-high islands up to completion of the first two monolayers. The population of bilayer islands is very sensitive to temperature and deposition rate, hence the controversy among several experiments regarding this growth mode.¹¹⁻¹⁴ From reflec-

tion high-energy electron-diffraction (RHEED) measurements of the in-plane lattice constant, May *et al.*¹⁰ infer a significant increase of the amount of bilayer islands upon increasing the deposition flux from 0.0042 to 0.056 ML/s at room temperature. At a fixed temperature of 330 K, Fassbender *et al.*⁹ observed a transition from bilayer growth at high flux ($F=0.3$ ML/s) to monolayer growth at low flux ($F=0.003$ ML/s). From other experiments it was also inferred that >300 K there is a transition to monolayer growth coupled with the exchange of Co atoms into the Cu surface.^{8,15-17} At room temperature, Kim *et al.*¹⁶ observe patches of pure Co and a Co/Cu surface alloy for deposition with $F=0.005$ ML/s. Co/Cu intermixing is coupled with the transition to monolayer growth at low-deposition fluxes in the study of Fassbender *et al.*⁹ Above 400 K a significant increase in the Cu population at the exposed surface up to 4.3 ML indicates activation of Cu segregation onto the surface via Co/Cu exchange processes, and at 450 K, Cu-capped Co layers are observed.³ The activation of Co/Cu surface exchange leads to non-Arrhenius behavior of the island density in the range 300–400 K, observed in both experimental¹⁵ and kinetic Monte Carlo (kMC) studies,¹⁸ and coexistence of large Co-decorated Cu islands and small Co islands on the surface.^{6,17} Co/Cu surface exchange can result in a variety of structures, such as a Co/Cu surface alloy,¹⁶ Cu-capped Co islands,³ and Co-decorated Cu islands.^{6,8,17}

Since experiments offer only indirect clues, the detailed kinetic mechanisms responsible for the various growth modes of Co/Cu are presently unknown. In the following, we combine static energy calculations with accelerated MD^{19,20} simulations using an empirical tight-binding second-moment approximation (TBSMA) potential function²¹ for describing the Co—Cu interaction to gain insight into atomic-level processes. We discover an upward-transport mechanism at island edges that is responsible for the bilayer island formation tendency at low temperatures. At higher

temperatures, the onset of Co/Cu exchange results in qualitatively different island morphologies and the upward transport mechanism is reversed, thereby promoting monolayer growth. Finally, we observe a high mobility of small Co clusters and analyze its impact on the submonolayer-regime growth.

II. ENERGETICS OF Co ON THE Cu(001) SURFACE USING EMPIRICAL POTENTIALS

Co and Cu interactions in our studies are based on the TBSMA potential of Levanov *et al.*²¹ This potential was constructed to fit experimentally determined lattice constants, cohesive energies and elastic constants for bulk Cu(fcc) and Co(hcp), as well as *ab initio* interaction energies for small Co clusters on Cu surfaces. Since we aim to compare our results to the DFT-kMC study of Pentcheva *et al.*,¹⁸ we slightly modify this TBSMA potential to obtain a better fit of their energetics. In the TBSMA formalism, the total energy E_{tot} of a system is the sum of a pair potential term E_P and a many-body term E_M ²¹

$$E_{\text{tot}} = E_P + E_M,$$

$$E_P = \frac{1}{2} \sum_{i,j=1}^N V_{\alpha\beta}(r_{ij}),$$


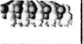
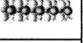
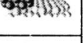
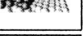
$$E_M = \sum_{i=1}^N F_{\alpha}(\rho_i), \quad \rho_i = \sum_{j=1}^N \rho_{\alpha\beta}(r_{ij}), \quad (1)$$

where N is the total number of atoms, $\alpha, \beta = \{\text{Co}, \text{Cu}\}$ are the two atom species, r_{ij} are interatomic distances, $V_{\alpha\beta}(r_{ij})$ is a pair potential, $\rho_{\alpha\beta}(r_{ij})$ is the “electronic density” generated by atom j at the location of atom i , and $F_{\alpha}(\rho_i)$ is the energy gained by embedding atom i in the total electronic density ρ_i . Following Haftel,²² the embedding functions can be altered at low electron densities without affecting bulk properties. For potentials fit mostly to the bulk, this improves the description of the strongly different environment experienced by surface atoms: for example, the electronic density ρ at the site of a surface atom is only 70% of the density ρ_0 in the bulk. Also, for single adatoms on surfaces and especially at transition states of diffusion processes (i.e., adatom hopping or exchange), the coordination is significantly decreased ($\rho \approx 0.25\rho_0$) and the remaining nearest-neighbor distances may be reduced to 80% of their bulk value. Here we modify both the embedding functions $F(\rho)$ below a threshold $\rho_{th} = 0.9\rho_0$ and the pair potentials $V(r)$ below a distance threshold $r_{th} = 0.9r_0^m$, where r_0^m is the nearest-neighbor distance in the bulk. For Cu, $r_0^m = 2.56 \text{ \AA}$, whereas for Co, $r_0^m = 2.50 \text{ \AA}$.²¹ We also apply a smooth cutoff at $r_c = 7 \text{ \AA}$, which is sufficient for preserving the correct energetics and the phase preference for Co(hcp) versus Co(fcc). We define “correction functions” $\delta V(r)$ and $\delta F(\rho)$ as cubic splines subject to the boundary conditions

$$\delta V(r) = \delta V'(r) = 0, \quad r \geq r_{th}$$

$$\delta F(\rho) = \delta F'(\rho) = 0, \quad \rho \geq \rho_{th}$$

TABLE I. Surface formation energies (eV/1×1 unit cell) for clean surfaces and various arrangements of 1 ML of Co on Cu(001). “TBSMA” values are obtained with the original potential of Ref. 21, “TBSMA[†]” values are obtained with our optimized potential. DFT values are taken from Ref. 6, except the (*) value which is from Ref. 23.

Structure	TBSMA	TBSMA [†]	DFT	Image
Cu(001)	0.55	0.58	0.61	
Co(001)	0.79	0.82	0.86 *	
Co/Cu	0.99	1.12	1.22	
Co/Cu alloy	0.90	1.03	1.09	
Cu/Co/Cu	0.73	0.87	0.99	
Co/Co/Cu	0.73	0.78	0.86	
Cu/2Co/Cu	0.66	0.72	0.73	

$$\delta F(0) = 0. \quad (2)$$

The new potential functions are

$$F_{\alpha}^{\text{new}}(\rho) = F_{\alpha}(\rho) + \delta F_{\alpha}(\rho),$$

$$V_{\alpha\beta}^{\text{new}}(\rho) = V_{\alpha\beta}(\rho) + \delta V_{\alpha\beta}(\rho), \quad \alpha, \beta = \{\text{Co}, \text{Cu}\}. \quad (3)$$

We construct the functions $\delta V(r)$ and $\delta F(\rho)$ by simulated annealing. The cost function to be minimized is

$$\mathcal{F}(\mathbf{x}) = \sum_j (E_j^{\text{new}} - E_j^{\text{DFT}})^2, \quad (4)$$

where E_j^{DFT} are the energies of the reference structures from Refs. 6 and 8, E_j^{new} are the energies obtained with our potential function, and \mathbf{x} is a multidimensional vector representing the values of the spline functions at the spline points $\{r_k, \rho_k\}$. Included in the fit are the surface formation energies shown in Table I (except the Co/Cu surface alloy) and energy barriers for Cu/Cu and Co/Cu hopping and exchange (shown in Table II). The surface energies are calculated for a 50-atom × 5-layer Cu slab subject to periodic boundary conditions along the coordinates parallel to the surface and covered on both faces by Co in various arrangements shown in Table I. As in Refs. 6 and 8, when the surface consists of two domains, the energy was calculated as a weighted sum of the formation energies of each domain. The modified embedding functions and Co—Cu pair potential are shown in Fig. 1.

Energy barriers^{6,23} from DFT and TBSMA calculations for several processes are shown in Table II. Of the values in Table II, only Cu/Cu hopping and Co/Cu hopping and exchange were included in the fitting procedure [Eq. (4)], along with surface formation energies. For fitting energy barriers to the DFT results, the energy E^{new} employed in Eq. (4) is

TABLE II. Energy barriers (electron volts) for elementary diffusion processes on the Cu and Co fcc(001) surfaces. “Step” barriers are for hopping along the close-packed Cu step oriented in the [110] direction. TBSMA values are calculated with the step-and-slide method.²⁴

Process	TBSMA ^a	TBSMA modified	DFT
Cu/Cu hop	0.44	0.48	0.51 ^b
Cu/Cu exchange	0.87	0.92	1.02 ^b
Co/Co hop	0.58	0.58	0.54 ^c
Co/Co exchange	1.32	1.48	1.54 ^b
Co/Cu hop	0.67	0.63	0.61 ^b
Co/Cu exchange	0.89	0.93	1.00 ^b
Co/Cu step	0.42	0.39	0.35 ^c

^aReference 21.

^bReference 6.

^cReference 23.

$$E^{\text{new}} = E_{\text{TS}} - E_{\text{LM}}, \quad (5)$$

where LM and TS denote the relaxed local minimum and transition-state structures, respectively. The main effect on energy barriers comes from modifying the transition-state energies by adjusting the pair potentials $V(r)$ at close distances of $r \approx 2.0$ Å and the embedding functions $F(\rho)$ at low electronic densities of $\rho \approx 0.2\rho_0$. As seen in Table II, we obtain a better fit of DFT barriers than the original potential²¹ where the Co/Cu hopping barrier was significantly overestimated, while all exchange processes and Cu/Cu barriers were underestimated.

III. SIMULATIONS OF Co/Cu(001) GROWTH

We perform accelerated molecular dynamics (MD) simulations of Co/Cu(001) growth using the state-bridging bond-boost method.^{19,20} We employ a simulation cell with five layers of Cu and lateral sizes from 400 to 1296 atoms/layer. We apply periodic boundary conditions in the directions parallel to the surface. The in-plane lattice constant is fixed to the Cu bulk value of $a_{\text{Cu}} = 3.615$ Å. The bottom two layers are immobile and fixed to ideal bulk positions. The middle layer is connected to a Nosé-Hoover thermostat²⁵ for controlling the temperature, whereas the top two layers follow Newton’s equations of motion for the microcanonical ensemble. We employ our version of the TBSMA potential, whose construction was described in Sec. II. Simulations are run in parallel on 1–16 processors of a Linux Athlon 1.5 GHz cluster with 100 Mbps ethernet network and the Penn State LionXM cluster with 3 GHz Pentium 4 processors and Myrinet interconnection network.

We simulate growth up to 0.5 ML, in a temperature range of 250–310 K and fluxes of 0.1–3 ML/s. For the accelerated MD algorithm¹⁹ all first-layer Cu atoms and the deposited Co atoms are included in the boost. The bond-stretch threshold for application of the boost potential is $\epsilon^{\text{max}} = 0.3$. The best efficiency is obtained with a boost amplitude of $\Delta V^{\text{max}} = 0.6$ eV (about the same as the isolated Co adatom

hop barrier), which allows for a speed-up of up to 10^8 at 250 K relative to conventional MD. As discussed in Ref. 20, the Co/Cu surface is a prime example of the “small-barrier problem,” i.e., it features processes occurring many orders-of-magnitude faster than ordinary adatom diffusion. Diffusion along step edges has barriers around 0.1–0.2 eV, which makes it 10^6 times faster than single adatom hopping in the temperature range probed here. In order to allow accelerated MD to reach the time scale of the slow events, we implement our shallow-state bridging algorithm.²⁰ We set the threshold barrier to $\Delta E^{\text{th}} = 0.4$ eV. This barrier separates the “slow” and “fast” time scales. After each event, we apply a low boost of $\Delta V^{\text{max}} = 0.2$ eV for a time t^{wait} , which is the average waiting time corresponding to the barrier ΔE^{th} and a prefactor of 10 ps^{-1} . The low boost allows correct dynamics of the fast events, which quickly settle to thermodynamic equilibrium. After the low-boost period t^{wait} we apply the high-boost amplitude $\Delta V^{\text{max}} = 0.6$ eV and effectively switch the simulation to the time scale of the slow events. The maximum physical time that can be simulated with the present method is on the order of a second at or below room temperature, which surpasses the window that has been probed in previous studies of thin-film epitaxy with accelerated MD.^{26,27} We emphasize that we can achieve these times because we employ a state-

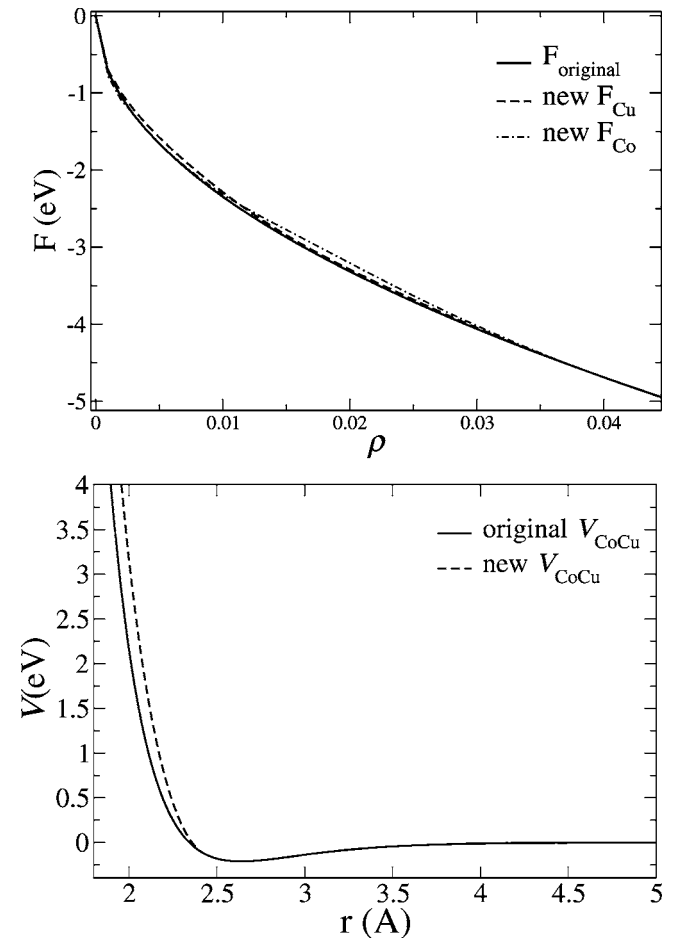


FIG. 1. Comparison of original (Ref. 21) and modified embedding functions for Co and Cu (top) and modified Co—Cu pair potential (bottom).

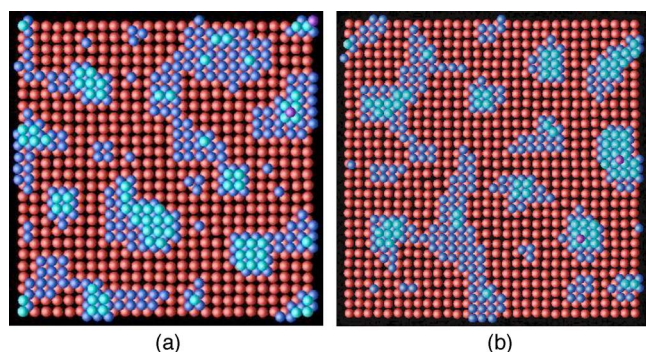


FIG. 2. (Color online) Surface morphology at $\theta=0.54$ for a flux of $F=0.1$ ML/s at $T=250$ K (a) and at $\theta=0.42$ for a flux of $F=1.0$ ML/s at $T=310$ K (b). Blue (dark-gray) atoms are first-layer Co and light-blue (light-gray) atoms are second-layer Co atoms. There are a few third-layer Co atoms, shown in purple (dark gray atop the light-gray atoms).

bridging accelerated MD algorithm.²⁰ Regular accelerated MD simulations^{28–32} would be limited by the fast times of small-barrier events associated with step-edge diffusion.

As discussed above, one intriguing feature observed experimentally for Co/Cu(001) is bilayer growth for coverages up to 2 ML below about room temperature.^{3,9–14} Using accelerated MD simulations, we observe the formation of bilayer islands at these conditions (cf., Fig. 2) and we find that bilayer island formation is enhanced by efficient *upward* mass transport at the edges of Co islands. Commonly, two-versus three-dimensional growth morphologies are explained in terms of the Ehrlich-Schwoebel barrier,³³ which hinders adatom hopping over island edges to lower layers in the growing film. However here, bilayer island formation is enhanced by adatoms *ascending* island edges.

We have performed an analysis of the energy barriers involved in bilayer-island formation. As implied by energetic considerations, Co seeks to maximize the number of Co–Co bonds at the expense of the weaker Co–Cu bonds by rearrangement of a 1 ML-island into a bilayer island. A Co adatom at the edge of a Co island will thus prefer to climb on top of the island with an energy gain of 0.25–0.35 eV, depending on the specific configuration at the step edge. This does not happen spontaneously due to a high barrier of around 0.9 eV. However, the presence of another Co atom on top of the island facilitates this process: the barrier for a corner Co atom to jump on top of the island is only 0.63 eV (as fast as single adatom hopping) for the process shown in Fig. 3(e). The barrier for descent for an isolated second-layer atom via exchange at a corner or kink is comparable [0.62 eV see Fig. 3(b)], whereas descent over a straight step edge has a very high Ehrlich-Schwoebel barrier [Fig. 3(a)]. This means that a Co adatom that has landed on top of a Co island will diffuse until it reaches a kink or corner, then, with almost equal probability, will either descend or pull up another Co atom from the edge onto the second layer. However, once a “nucleus” of two Co atoms is formed on top of a Co island, the downward mass transport is frozen, being both thermodynamically and kinetically inconvenient [Fig. 3(c)]. At the same time, upward mass transport continues and

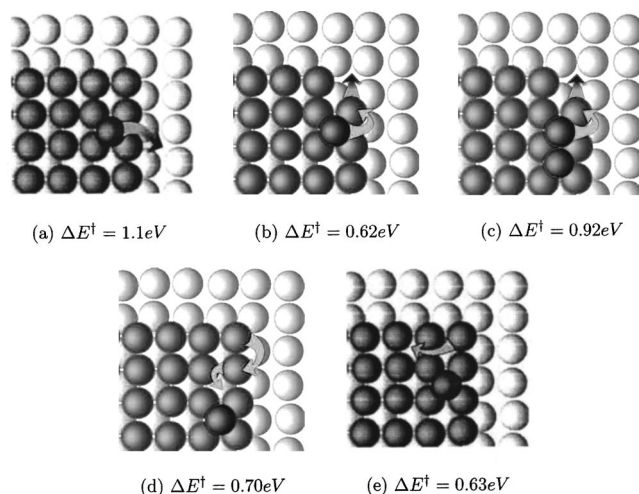


FIG. 3. Interlayer transport barriers for Co islands on Cu(001): (a)–(c) downward; (d) and (e) upward. These barriers were obtained via static calculations with the step-and-slide method.²⁴ Cu surface atoms are white, first-layer Co atoms are gray, and second-layer Co atoms are dark gray. The respective processes are indicated by the arrows.

more atoms are pulled up from the edges by the increasing second-layer nucleus. A sample simulation of a Co adatom on top of a 72-atom Co island was carried out at $T=330$ K. The adatom diffuses until it reaches the corner, where it pulls up an edge Co and the process continues until, 10 ms after deposition, a total of seven atoms are pulled up from the edge. The start and end points of the simulation are shown in Fig. 4.

Atoms from upward mass transport make up a significant portion of second-layer Co atoms during growth. We carried out simulations of deposition of 0.42 ML at $T=310$ K and fluxes in the range of 0.5–3 ML/s. In Fig. 5 we plot the fraction θ_2/θ_1 of the deposited Co atoms that are in the second layer and the fraction θ_2^{1-2}/θ_2 of the second-layer atoms resulting from upward transport, where θ_i indicates the absolute coverage of the i th deposited layer. The ratio θ_2/θ_1 increases approximately linearly with the deposition flux F . Thus, for a higher flux more atoms are in the second layer at

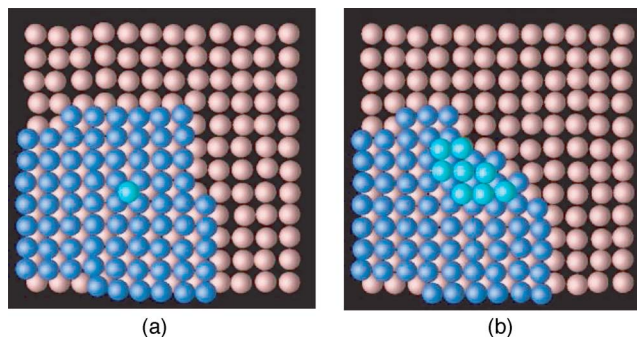


FIG. 4. (Color online) Initial (a) and final (b) configurations for an accelerated MD simulation of a deposition event of Co on a Co island at $T=330$ K. Simulated time=10 ms. First-layer Co atoms are blue (dark gray) and second-layer Co atoms are light blue (light gray).

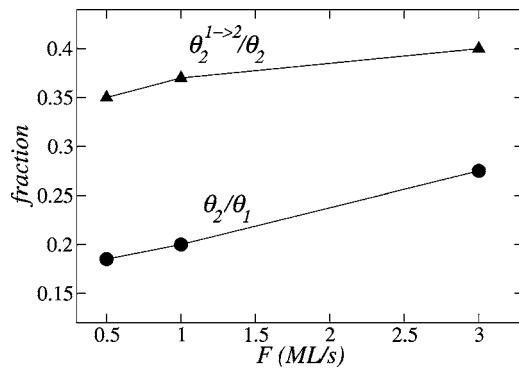


FIG. 5. Fractional filling of the second Co layer at $T=310$ K and total coverage $\theta=\theta_1+\theta_2=0.42$ ML, where θ_i is the coverage of layer i . $\theta_2^{1 \rightarrow 2} / \theta_2$ is the fraction of the material in the second layer resulted from upward transport from the first layer.

a fixed coverage. This is an influence of the average island size: a higher flux produces a larger number of smaller islands. An adatom that is deposited on top of a small island is very close to a corner or kink, thus the “attempt frequency” for the upward-transport process is high. On the other hand, a low flux results in fewer, larger islands. An atom that has landed on top of a large island must diffuse further to reach a corner, where it will either descend or pull up another Co atom. During this time, there is a higher probability that other atoms will land on top of the same island and that they will form a stable, less mobile nucleus, which does not reach the island edge. Thus the fraction of second-layer atoms that arrived there by upward transport from the first layer is lower. Also, for a large island the impact of upward transport will be only manifested at the edges. The sample simulation in Fig. 4 shows that for a large island the upward transport stops after a bilayer-high “wall” is formed around the island edge. Since the center of the island remains monolayer high, the fraction θ_2 / θ_1 is expected to be lower with increasing island size (i.e., decreasing flux). The upward transport discovered through MD simulations explains the experimental findings of Fassbender *et al.*,⁹ where at a temperature $T=330$ K and flux $F=0.3$ ML/s bilayer-high island edges surrounding monolayer-high island centers are observed.

At higher temperatures ($T \geq 350$ K) and lower deposition fluxes ($F \leq 0.005$ ML/s), it is observed experimentally that the bilayer growth mode disappears in favor of monolayer-high island formation.⁹ We found that the explanation lies in the *qualitative* change in the island structure stemming from the activation of exchange processes. Co/Cu exchange has a barrier of 0.92 eV (TBSMA), which means that above room temperature, exchange processes happen on a time scale of less than a second. Co/Cu exchange is irreversible and Co atoms embedded in the first Cu layer become immobile pinning centers that lead to the formation of small Co islands. On the other hand, Cu atoms released on the surface after Co/Cu exchange have a much higher mobility than Co. They form large Cu islands, decorated at the edges by the slower Co adatoms.^{6,17}

We find that the qualitative change in surface morphology effectively reverses interlayer transport. Activation barriers for step ascent and descent for a large, Co-decorated Cu

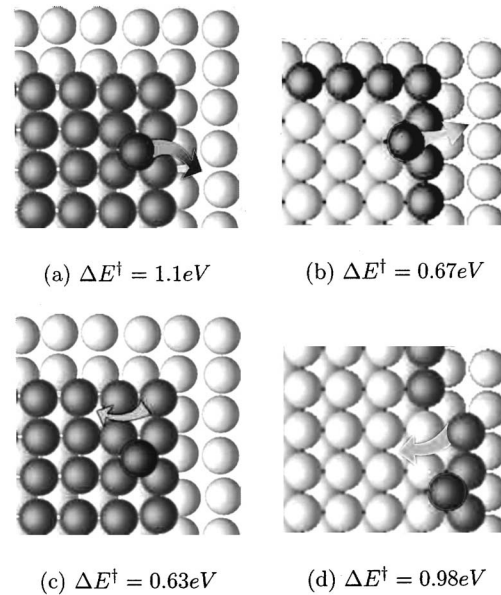


FIG. 6. Comparison of downward (a and b) and upward (c and d) interlayer transport barriers for a pure Co island (a and c) vs Co-decorated Cu island (b and d). Barriers were statically calculated with the step-and-slide method.²⁴ Cu surface atoms are white, first-layer Co atoms are gray and second-layer Co atoms are dark gray. The respective processes are indicated by the arrows.

island are shown in Fig. 6. Since the first adatom layer is formed mainly by Cu, Co gains no energy by jumping on top of an island. Hence the upward diffusion at island corners is “deactivated” because of the high barrier of 0.98 eV (up from 0.62 eV for a pure Co island). At the same time, the Ehrlich-Schwobel barrier for step descent is reduced to 0.67 eV. Also, the mobility of Co upon reaching the Co edge of the Cu island is reduced: hopping along the Co-decorated island edge has a barrier of 0.7 eV, which makes it slower than terrace diffusion and edge descent. Thus, a Co adatom on top of a Co-decorated Cu island diffuses until reaching an island edge, where it sticks to the edge Co atoms. Due to a weak Ehrlich-Schwobel barrier, the adatom will eventually hop over the edge. Accelerated MD simulations of Co atoms on top of Co-decorated Cu islands confirm this picture. The mixed island composition inhibits upward mass transport, while it strongly promotes downward diffusion, leading to layer-by-layer growth.

In addition to complex interlayer transport mechanisms, the growth of Co on Cu(001) exhibits another interesting phenomenon: a significant mobility of small clusters. As discussed in Ref. 20, Co clusters of up to seven atoms have a mobility comparable to isolated Co adatoms. The trimer hops via a concerted jump of two atoms, while the heptamer hops via concerted shearing of three atoms in the middle row. These processes are shown in Table III. A partial explanation for such small barriers is the strong “inward” relaxation of small Co islands (see also Refs. 4 and 5). For the Co dimer, the Co–Co distance is 2.4 Å regardless of whether the dimer is oriented along the [110] or [100] direction, which means in the latter case an inward relaxation of 34% compared to the second-neighbor lattice spacing of the Cu lattice. There is

TABLE III. Static energy barriers ΔE for cluster diffusion processes of Co/Cu(001). See Ref. 20 for a more detailed explanation of these processes.

Process	ΔE (eV)
Dimer hop	0.62
Adatom edge hop	0.20
Trimer rotation	0.10
Trimer hop	0.64
Heptamer hop	0.56

also a strong relaxation for the Co trimer: the Co–Co second-neighbor distance is 3.1 Å, a 14% relaxation from the ideal lattice position. The strong relaxation means there is less Co–Co “bond-breaking” at transition states (TS): for the Co dimer, the Co–Co nearest-neighbor bond remains intact at the TS, hence the energy barrier for dimer hopping reflects mostly the adatom-substrate interaction and is the same as the isolated adatom hopping barrier.

The efficiency of multiatom, small-cluster diffusion processes challenges the validity of kMC studies of growth,^{6,17,18} where only single-adatom terrace and edge diffusion are taken into account. Although obtaining a correct qualitative agreement with experiments, the kMC simulations in Refs. 6 and 18 result in average island densities larger by a factor of 2 than the experimental values. In these simulations, clusters are considered immobile except for small diffusivity resulting from adatom motion along island edges. Lately, theoretical and simulation results indicate that mobility of small clusters may have a significant effect on growth morphology.^{34–36}

Typically, growth and nucleation of islands in the sub-monolayer regime is characterized by the mean island density N_{av} (islands/unit cell) and the island-size distribution. The mean-field scaling theory^{37,38} for isotropic two-dimensional surface growth is based on the assumption of a critical cluster size i above which islands do not dissociate and includes diffusion via single adatom hopping rates h_1 , but ignores cluster mobility. In the case where dimers are stable ($i=1$), the predicted saturation N_{av} scales with deposition flux F and temperature T as

$$N_{av} \sim \left(\frac{F}{h_1}\right)^{1/3}. \quad (6)$$

However, if dimers and other clusters become significantly mobile relative to the single adatom, the above scaling does not hold. Villain *et al.*³⁴ have shown that, if dimers have a hopping rate h_2 , the scaling of N_{av} is modified to

$$N_{av} \sim \left(\frac{F^2}{h_1 h_2}\right)^{1/5}. \quad (7)$$

Equation (7) holds for sufficiently large h_2 and h_1/F . Bartelt *et al.*³⁶ showed that the transition to the modified scaling in Eq. (7) is controlled by the dimensionless parameter Z

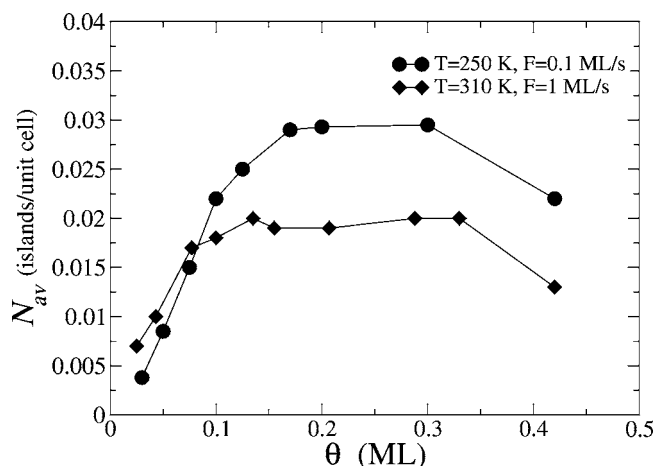


FIG. 7. Variation of island density N_{av} with the coverage θ during accelerated MD simulations of Co/Cu(001) growth.

$=(h_2/F)^3(h_1/F)^{-2}$. For $Z \ll 1$, dimer mobility has no effect on N_{av} , whereas Eq. (7) holds for $Z \gg 1$.

For Co/Cu(001) growth, dimer and adatom diffusion have essentially equal energy barriers, hence $h_1 \approx h_2$ and Eq. (7) becomes

$$N_{av} \sim \left(\frac{F}{h_1}\right)^{2/5}. \quad (8)$$

The theory then predicts the 2/5 scaling to replace the 1/3 scaling in Eq. (6) for $h_1/F \gg 1$. We probed the effect of cluster diffusion using accelerated MD for direct comparison with the kMC study of growth in Ref. 18. We simulated growth up to 0.5 ML at $\{T=250$ K, $F=0.1$ ML/s $\}$ and $\{T=310$ K, $F=1$ ML/s $\}$. To obtain reliable statistics, we employed a large simulation cell of 1296 atoms/layer for the low temperature and 900 atoms/layer for the high temperature. The variation of the island density with coverage is plotted in Fig. 7, which indicates that it reaches the saturation value at about 0.2 ML coverage. In these regimes, $h_1/F \approx 250$ at $T=250$ K and $h_1/F \approx 900$ at $T=310$ K, which means the dimer mobility should have a significant effect, cf., Eq. (8). For the same set of parameters $\{T=250$ K, $F=0.1$ ML/s $\}$ and accounting for the small adatom hopping barrier difference (0.02 eV) between the DFT and TBSMA values, we obtain $N_{av}^{\text{MD}} = 0.7 N_{av}^{\text{kMC}}$, i.e., cluster mobility results in a 30% decrease of the island density N_{av} compared to the “immobile cluster” assumption employed in the kMC simulations of Ref. 18. The result agrees with the mean-field theory, which predicts a 26% decrease of N_{av} if dimer mobility is considered [the value results from comparing Eqs. (8) and (6)]. At $T=310$ K we used a flux of $F=1$ ML/s, which is 10 times higher than the kMC flux. Since N_{av}^{kMC} satisfies Eq. (6), we can rescale the kMC value to obtain the island density corresponding to $F=1$ ML/s. In this way we also obtain a 34% decrease in the island density compared to the (rescaled) kMC value from Ref. 18. The significant decrease in island density because of cluster mobility may be the most important reason for the discrepancy between experimental measurements and kMC simulations of

Co/Cu(001) growth,¹⁸ which consistently predict island densities larger by a factor of two than experimental observations. Our simulations show that including cluster diffusion in kMC simulations could eliminate the discrepancy.

IV. CONCLUSIONS

Although accelerated MD simulations can be computationally demanding, these simulations offer an unprecedented power for probing experimental temperature and time scales in a “prejudice-free” manner. We perform accelerated MD simulations that are able to cover time scales of seconds at or close to room temperature, thereby bringing the domain of experimental observations within the reach of accurate simulation tools. We are able to probe such time scales through use of our state-bridging algorithm,²⁰ which consolidates groups of minima connected by small barriers into large minima, thereby eliminating the kinetic treatment of

the fast motion, so that long-time motion can be probed. For Co/Cu(001) growth in the regime where surface exchange is inactive, an upward interlayer transport mechanism was found to contribute to the bilayer growth mode. At higher temperatures, with the onset of Co/Cu surface exchange, the mixed island composition inhibits upward transport of Co adatoms while promoting descent at island edges, leading to monolayer growth. We also show that small island diffusion through concerted atomic mechanisms brings about a significant lowering of the saturation island density as compared to kMC calculations where concerted mechanisms were ignored, and including this correction into kMC will likely eliminate the discrepancy between experimental and kMC simulation results.

ACKNOWLEDGMENT

This work was funded by NSF Grant No. ECC-0085604.

-
- ¹R. Pasianot and E. J. Savino, *Phys. Rev. B* **45**, 12704 (1992).
²S. M. Foiles, M. I. Baskes, and M. S. Daw, *Phys. Rev. B* **33**, 7983 (1986).
³M. T. Kief and W. F. Egelhoff, *Phys. Rev. B* **47**, 10785 (1993).
⁴V. Stepanyuk, D. Bazhanov, A. Baranov, W. Hergert, A. Katsnelson, P. Dederichs, and J. Kirschner, *Appl. Phys. A: Mater. Sci. Process.* **72**, 443 (2001).
⁵V. S. Stepanyuk, D. I. Bazhanov, W. I. Hergert, and J. Kirschner, *Phys. Rev. B* **63**, 153406 (2001).
⁶R. Pentcheva, Ph.D. thesis, Freie Universität Berlin (2000).
⁷B. Drittler, M. Weinert, R. Zeller, and P. H. Dederichs, *Phys. Rev. B* **39**, 930 (1989).
⁸R. Pentcheva and M. Scheffler, *Phys. Rev. B* **61**, 2211 (2000).
⁹J. Fassbender, R. Allenspach, and U. Dürig, *Surf. Sci.* **383**, L742 (1997).
¹⁰U. May, J. Fassbender, and G. Güntherodt, *Surf. Sci.* **377–379**, 992 (1997).
¹¹H. Li and B. Tonner, *Surf. Sci.* **237**, 141 (1990).
¹²S. Ferrer, E. Vlieg, and I. Robinson, *Surf. Sci. Lett.* **250**, L363 (1991).
¹³A. Schmid and J. Kirschner, *Ultramicroscopy* **42–44**, 483 (1992).
¹⁴U. Ramsperger, A. Vaterlaus, P. Pfäffli, U. Maier, and D. Pescia, *Phys. Rev. B* **53**, 8001 (1996).
¹⁵T. Bernhard, R. Pfandzelter, and H. Winter, *Nucl. Instrum. Methods Phys. Res. B* **203**, 111 (2003).
¹⁶S. Kim, J. Kim, J. Han, J. Seo, C. Lee, and S. Hong, *Surf. Sci.* **453**, 47 (2000).
¹⁷F. Nouvertné, U. May, M. Bamming, A. Rampe, U. Korte, G. Güntherodt, R. Pentcheva, and M. Scheffler, *Phys. Rev. B* **60**, 14382 (1999).
¹⁸R. Pentcheva, K. A. Fichthorn, M. Scheffler, T. Bernhard, R. Pfandzelter, and H. Winter, *Phys. Rev. Lett.* **90**, 076101 (2003).
¹⁹R. Miron and K. Fichthorn, *J. Chem. Phys.* **119**, 6210 (2003).
²⁰R. A. Miron and K. A. Fichthorn, *Phys. Rev. Lett.* **93**, 128301 (2004).
²¹N. A. Levanov, V. S. Stepanyuk, W. Hergert, D. I. Bazhanov, P. H. Dederichs, A. A. Katsnelson, and C. Massobrio, *Phys. Rev. B* **61**, 2230 (2000).
²²M. I. Haftel, *Phys. Rev. B* **48**, 2611 (1993).
²³Y. Shin and M. Scheffler (private communication).
²⁴R. Miron and K. Fichthorn, *J. Chem. Phys.* **115**, 8742 (2001).
²⁵W. G. Hoover, *Phys. Rev. A* **31**, 1695 (1985).
²⁶F. Montalenti, M. R. Sørensen, and A. F. Voter, *Phys. Rev. Lett.* **87**, 126101 (2001).
²⁷J. A. Sprague, F. Montalenti, B. P. Uberuaga, J. D. Kress, and A. F. Voter, *Phys. Rev. B* **66**, 205415 (2002).
²⁸A. Voter, *J. Chem. Phys.* **106**, 11 (1997).
²⁹A. F. Voter, *Phys. Rev. Lett.* **78**, 3908 (1997).
³⁰A. Voter, *Phys. Rev. B* **57**, R13985 (1998).
³¹M. M. Steiner, P.-A. Gerrilloud, and J. W. Wilkins, *Phys. Rev. B* **57**, 10236 (1998).
³²S. Pal and K. Fichthorn, *Chem. Eng. J.* **74**, 77 (1999).
³³R. Schwoebel, *J. Appl. Phys.* **40**, 614 (1969).
³⁴J. Villain, A. Pimpinelli, L. Tang, and D. Wolf, *J. Phys. I* **2**, 2107 (1992).
³⁵S. Liu, L. Bönig, and H. Metiu, *Phys. Rev. B* **52**, 2907 (1995).
³⁶M. C. Bartelt, S. Günther, E. Kopatzki, R. J. Behm, and J. W. Evans, *Phys. Rev. B* **53**, 4099 (1996).
³⁷J. Venables, G. Spiller, and M. Hanbücken, *Rep. Prog. Phys.* **47**, 399 (1984).
³⁸M. C. Bartelt and J. W. Evans, *Phys. Rev. B* **46**, 12675 (1992).